Kinetics, selectivity and scale up of the Fischer-Tropsch synthesis

van der Laan, Gerard Pieter

4

α-Olefin Readsorption Product Distribution Model for the Gas-Solid Fischer-Tropsch Synthesis

Abstract

The kinetics of the gas-solid Fischer-Tropsch synthesis over a commercial Fe-Cu-K-SiO_2 catalyst was studied in a continuous spinning basket reactor. Experimental conditions were varied as follows: reactor pressure of 0.8-4.0 MPa, H_2/CO feed ratio of 0.25-4.0, and space velocity of 0.5-2.0 10^{-3} Nm^3 kg_{cat}^{-1} s^{-1} at a constant temperature of 523 K. A new product distribution model for linear hydrocarbons is proposed. Deviations from conventional Anderson-Schulz-Flory distribution can be quantitatively described with an α-Olefin Readsorption Product Distribution Model. The experimentally observed relatively high yield of methane, relatively low yield of ethene and both the exponential decrease of the olefin to paraffin ratio and the change of the chain growth parameter with chain length can all be predicted from this new model. It combines a mechanistic model of olefin readsorption with kinetics of chain growth and termination on the same catalytic sites. The hydrocarbon formation is based on the surface carbide mechanism by CH_2 insertion. The olefin readsorption rate depends on chain length due to increasing physisorption strength on the catalyst surface and increasing solubility in FT-wax inside the catalyst pores with increasing chain length. Interfacial concentrations of reactive olefins near the gas-wax and wax-catalyst surface are used in the kinetic model. By optimizing three parameters per experimental product distribution, the olefin readsorption product distribution model proved to predict product selectivities accurately over the entire range of experimental conditions. The relative deviations are 10.1 % and 9.1 % for the selectivity to paraffins and olefins with carbon number smaller than 11, respectively.

4.1 Introduction

The FT synthesis has been recognized as a polymerization reaction [1]. The reactants, CO and H_2, adsorb and dissociate at the surface of the catalyst and react to form chain initiator (CH_3), and methylene monomer (CH_2) and H_2O. The most important growth mechanism for the hydrocarbon formation is the surface carbide mechanism by CH_2 insertion into adsorbed alkyl chains. Termination can take place by dehydrogenation to an α-olefin or hydrogenation to form a paraffin [2–4].

The product yield decreases exponentially with increasing chain length. The so-called Anderson-Schulz-Flory (ASF) distribution describes the entire product range by a single parameter, α, the probability of the addition of a carbon intermediate to a chain [2, 5]. However, significant deviations from the ASF distribution are reported in literature. The usual deviations of the distribution of α-olefins and paraffins are a relatively high yield of methane [6–9] and a relatively low yield of ethene [6, 7, 10] in comparison to the ASF distribution. Higher surface mobility or reactivity of C_1 and C_2 precursors and rapid readsorption of ethene give the most reasonable explanation for the deviations of the short-chain hydrocarbons from the ASF distribution (Chapter 2). Furthermore, an exponential decrease of the α-olefin to paraffin ratio and change in chain growth parameter, α_n, with increasing chain length is observed. These deviations are caused by secondary reactions, readsorption and hydrogenation, of α-olefins [7, 11–13]. However, secondary hydrogenation is strongly inhibited by CO and H_2O in comparison to readsorption [12]. Readsorption of α-olefins leads to chain initiation and will result in a decrease of the olefin to paraffin ratio and increase of the chain growth parameter with chain length. The olefin readsorption rate depends on chain length due to increasing physisorption on the catalyst surface and increasing solubility in FT-wax with chain length [7, 13].

Models for the hydrocarbon selectivity of products obtained on iron catalysts are usually based on the ASF distribution; the total hydrocarbon yield is calculated with a single chain growth factor, α [2, 14]. The ”break” or increase of the chain growth factor in the ASF distribution of the total hydrocarbon yield was observed on iron catalysts [15–20]. Some authors described the total hydrocarbon yield with two different catalytic sites with different chain growth probabilities, since the total hydrocarbon distribution could be fitted by addition of two individual ASF distributions [19, 20]. However, such double-α models cannot explain the decrease of the olefin to paraffin ratio.

More comprehensive models taking into account the readsorption of olefins during

the FT synthesis have been published, mostly for non-iron catalysts only. Zimmerman et al. [21] proposed a kinetic model for both the formation of linear olefins and paraffins and for the water gas shift reaction over iron catalysts. Their model takes into account olefin readsorption on FT sites and secondary hydrogenation of olefins on separate hydrogenation sites. Their model predicts a decrease of the olefin to paraffin ratio and an increase of the chain growth factor with increasing carbon number. The decrease of the olefin content is ascribed to high olefin concentrations in the liquid phase. However, the model was tested for one experiment only and showed significant deviations between model prediction and experimental mole fractions, specially for methane and ethene. The major differences between the new model proposed here and the model of Zimmerman et al. [21] will be discussed below. The model of Iglesia and co-workers, see for example Iglesia et al. [12], is based on diffusion-enhanced olefin readsorption due to a decrease of diffusion coefficients with increasing carbon number. As discussed below, it is more likely that preferential physisorption and increase of the solubility with increasing chain length result in a high surface concentration of adsorbed olefins. Komaya and Bell [7] measured the dynamic and steady-state Fischer-Tropsch synthesis over Ru/TiO_2 and determined the pseudo reaction rate constants of the chain growth, termination, and readsorption of olefins. The authors accounted for the effect of chain length dependent readsorption of olefins due to increasing physisorption with increasing carbon number, as well as depolymerization of ethene and dehydrogenation of methyl. However, they did not specify separate termination reactions for the formation of paraffins and olefins from adsorbed alkyl species, but lumped these termination reactions in a single termination rate constant. Therefore, no complete description of the product distribution could be obtained using their model. Kuipers et al. [13] modeled experimental data of the olefin to paraffin ratio synthesized on wax-coated and uncoated cobalt foils at low CO conversions at atmospheric pressures and a temperature of 493 K. Their model predicts an exponential decrease of the olefin to paraffin ratio with carbon number due to increased physisorption and solubility with increasing chain length. This model was extended by Kuipers et al. [9] in order to incorporate hydrogenation and cracking on Co/SiO_2 wafers and Co foils. In contrast to Kuipers et al. [13], they concluded that the deviations from the ASF distribution on Co foils were completely due to hydrogenation instead of readsorption of olefins.

The aim of this chapter is to develop and test a new product distribution model, called α-Olefin Readsorption Product Distribution Model (ORPDM) based on the results of kinetic experiments at industrially relevant conditions over a precipitated iron

catalyst to explain the deviations from the ASF distribution. The new model combines a mechanistic model of olefin readsorption with kinetics of chain growth and termination on the same catalytic sites. In this chapter, the emphasis is placed on the selectivity to linear olefins and paraffins.

4.2 α-Olefin Readsorption Product Distribution Model

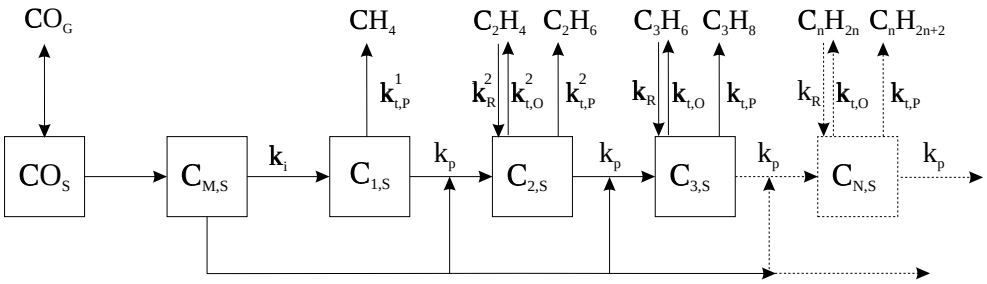

Figure 4.1 Reaction network α-Olefin Readsorption Product Distribution Model. The model reduces to ASF model when k_R^2, and $k_R = 0$.

The α-Olefin Readsorption Product Distribution Model (ORPDM) accounts for secondary readsorption of α-olefins on FT growth sites on the precipitated iron catalyst (see Figure 4.1). Here, CO_G and CO_S denote the gas phase and the adsorbed CO, respectively. $C_{M,S}$ refers to adsorbed monomeric building units ($CH_{2,s}$), and $C_{n,S}$ is an adsorbed alkyl species with carbon number n. Conversion of CO to $C_{M,S}$ follows a sequence of elementary reaction steps, but is shown as a single step. Table 4.1 shows the reactions for the chain growth and termination of alkyl chains. Chain growth initiates by hydrogenation of $C_{M,S}$ to $CH_{3,S}$, while chain propagation proceeds via insertion of $C_{M,S}$ into adsorbed alkyl chains. Chain termination by dehydrogenation of adsorbed alkyl chains gives olefins, whereas paraffins are formed by hydrogenation of alkyl species [7, 22]. Based on the reaction network shown in Figure 4.1, α-olefins may readsorb on growth sites and continue to grow via propagation with monomers or terminate as hydrocarbon product [7, 11].

Steady state mass balances for C_2 and alkyl species with carbon number, n, can be derived to account for readsorption:

$$k_p\theta_M\theta_1 = (k^2_{t,O}\theta_v + k^2_{t,P}\theta_H + k_p\theta_M)\theta_2 - k^{2*}_R C_{C_2H_4} \tag{4.1}$$

$$k_p\theta_M\theta_{n-1} = (k_{t,O}\theta_v + k_{t,P}\theta_H + k_p\theta_M)\theta_n - k^*_R C_{C_nH_{2n}} \tag{4.2}$$

Table 4.1 Proposed mechanism of the chain growth and termination reactions [3, 11].

	Elementary reactions	Reaction rates
1	$H_2 + 2s \rightleftarrows 2Hs$	
2[1]	$CO + 2H_2 + s \rightarrow CH_2s + H_2O$	
3	$CH_2s + Hs \rightarrow CH_3s + s$	
4	$CH_3s + Hs \rightarrow CH_4 + 2s$	$k^1_{t,P}\theta_1\theta_H$
5	$CH_3s + CH_2s \rightarrow C_2H_5s + s$	$k_p\theta_1\theta_M$
6	$C_2H_5s + s \rightleftarrows C_2H_4 + Hs + s$	$k^2_{t,O}\theta_2\theta_v - k^2_R C_{C_2H_4}\theta_H\theta_v$
7	$C_2H_5s + Hs \rightarrow C_2H_6 + 2s$	$k^2_{t,P}\theta_H\theta_2$
8	$C_2H_5s + CH_2s \rightarrow C_3H_7s + s$	$k_p\theta_2\theta_M$
9	$C_nH_{2n+1}s + s \rightleftarrows C_nH_{2n} + Hs + s$	$k_{t,O}\theta_n\theta_v - k_R C_{C_nH_{2n}}\theta_H\theta_v$
10	$C_nH_{2n+1}s + Hs \rightarrow C_nH_{2n+2} + 2s$	$k_{t,P}\theta_n\theta_H$
11	$C_nH_{2n+1}s + CH_2s \rightarrow C_{n+1}H_{2n+3} + s$	$k_p\theta_n\theta_M$
	etc.	

[1] Overall reaction for methylene formation.

where θ_H is the surface coverage of adsorbed hydrogen and θ_v is the fraction of vacant catalytic sites, and $k^*_R = k_R\theta_v\theta_H$ is a pseudo kinetic constant for the readsorption path. Since the readsorption reaction path of olefins is built up from several consecutive elementary surface reactions it is simplified as a single kinetic reaction rate constant (k^*_R). The actual concentration of the olefin on the catalyst surface, $C_{C_nH_{2n}}$, can be related to the reaction rate:

$$R_{C_nH_{2n}} = k_{t,O}\theta_v\theta_n - k^*_R C_{C_nH_{2n}} \tag{4.3}$$

It is assumed that the olefins leave the reactor in the gas phase. The same assumption was made by Iglesia et al. [11] and Kuipers et al. [13]. Liquid products are predominantly paraffins, which are unreactive under Fischer-Tropsch conditions. The steady-state mass balance for α-olefins in an ideally mixed continuous reactor is

$$R_{C_nH_{2n}} = \frac{\Phi_{v,R}P_{C_nH_{2n}}}{WRT} \tag{4.4}$$

where $P_{C_nH_{2n}}/RT$ is the gas phase concentration of olefins in the reactor with carbon number n, $\Phi_{v,R}$ is the volumetric flow rate of the gas phase at reactor conditions, and W is the weight of the unreduced supported catalyst.

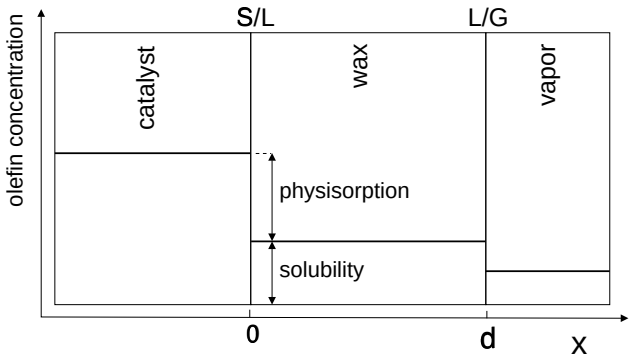

Figure 4.2 Olefin concentration profile near a Fischer-Tropsch catalyst.

The interfacial effects of reactive olefins at the gas-wax and wax-catalyst surface should be taken into account. Figure 4.2 gives a schematic representation of the olefin concentration profile in a wax-filled catalyst pore. The concentration in the wax phase (at $0 \leq x \leq d$) can be related to the vapor-phase concentration by Henry's law. Several authors stated that a greater solubility of larger hydrocarbons results in an increase of readsorption rates for larger olefins [13, 23, 24]. Vapor-liquid equilibria [25–28] show that the solubility of hydrocarbons increases exponentially with the chain length.

Data on the adsorption of hydrocarbons on solids show that the enthalpy of adsorption increases linearly with carbon number [29–31]. Adsorption equilibria constants increase exponentially with chain length [7, 30, 32, 33]. This increase results from an increase of the contact area between hydrocarbons and catalytic surface, which enhance Van der Waals attraction forces responsible for physisorption effects. Since physisorption is the precursor step to chemisorption, this increase is essential for readsorption of olefins. In multi-component mixtures (Fischer-Tropsch product spectrum) these effects result in a physisorbed layer with mainly long-chain hydrocarbons, while shorter chains are further away from the surface.

Iglesia and co-workers studied the influence of chain-length dependent diffusion coefficients on secondary reactions [11, 12, 34–37]. They reported an empirical equation describing a strong influence of chain length on diffusivity for olefins and paraffins $D_n \propto e^{-0.3n}$, which was not verified by experimental data. This carbon number dependency is a factor of three higher than experimentally determined by Erkey et al. [38]. Furthermore, the Wilke-Chang correlation [39] predicts a chain length dependence proportional to $n^{-0.5}$. Therefore, increase of readsorption rates of olefins with

chain length can hardly be due to diffusion effects only. More likely, preferential physisorption and increase of the solubility with chain length result in a high surface concentration of adsorbed olefins. Therefore we assume the olefin gas phase pressure to relate to the concentration at the catalyst surface as:

$$\frac{C_{C_nH_{2n}}}{P_{C_nH_{2n}}/RT} \propto e^{c\ n} \tag{4.5}$$

where c is a constant depending on the exponential increase of the physisorption and solubility with chain length.

Rearranging and solving eqs 4.1 - 4.5 yields:

$$\frac{\theta_2}{\theta_1} = \frac{k_p\theta_M}{k_{t,O}^2\theta_v/\left(1+k_R^2\right)+k_{t,P}^2\theta_H+k_p\theta_M} = \frac{p}{t_O^2/\left(1+k_R^2\right)+t_P^2+p} = \alpha_2 \tag{4.6}$$

and for $n > 2$:

$$\frac{\theta_n}{\theta_{n-1}} = \frac{k_p\theta_M}{k_{t,O}\theta_v/\left(1+k_Re^{c\ n}\right)+k_{t,P}\theta_H+k_p\theta_M} = \frac{p}{t_O/\left(1+k_Re^{c\ n}\right)+1+p} = \alpha_n \tag{4.7}$$

where $k_R = k_R^* WP/(\Phi_{v,0}P_0)$ (P= reactor pressure and $\Phi_{v,0}$= flow rate at normal conditions), $p = k_p\theta_M/k_{t,P}\theta_H$, $t_P^2 = k_{t,P}^2/k_{t,P}$, and $t_O^2 = t_P^2 t_O$, and $t_O = k_{t,O}\theta_v/k_{t,P}\theta_H$. These model parameters are pseudo kinetic rate constants, incorporating true kinetic rate constants, surface concentrations and process conditions. The surface fractions of alkyl chains with carbon number n can be determined by successive calculation of the chain growth parameter with increasing carbon number:

$$\frac{\theta_n}{\theta_1} = \prod_{i=2}^{n}\alpha_i = \alpha_2\ \alpha_3\ \cdots\alpha_n \tag{4.8}$$

The formation rate of paraffins with $n > 2$ (see Table 4.1) is equal to:

$$R_{C_nH_{2n+2}} = k_{t,P}\theta_H\theta_n \tag{4.9}$$

Normalizing eq 4.9 with respect to the termination to paraffins and substitution of eq 4.8 yields:

$$m_{C_nH_{2n+2}} = \theta_1\prod_{i=2}^{n}\alpha_i \tag{4.10}$$

Similarly, solving eqs 4.3 and 4.4 gives the following reaction rates and molar selectivities for olefins:

$$R_{C_nH_{2n}} = \frac{k_{t,O}\theta_v\theta_n}{1 + k_R e^{c\ n}} \tag{4.11}$$

$$m_{C_nH_{2n}} = \frac{t_O}{1 + k_R e^{c\ n}}\theta_1 \prod_{i=2}^{n} \alpha_i \tag{4.12}$$

The selectivity to product i is calculated from the experimental mole fractions relative to all products (n) considered:

$$m_i = \frac{y_i}{\sum_{j=1}^{n} y_j} \tag{4.13}$$

The molar selectivities of the C_1 and C_2 products are calculated differently:

$$m_{CH_4} = t_P^1\theta_1 \tag{4.14}$$

$$m_{C_2H_6} = t_P^2\theta_2 = t_P^2\alpha_2\theta_1 \tag{4.15}$$

$$m_{C_2H_4} = \frac{t_O^2}{1 + k_R^2}\theta_2 \tag{4.16}$$

with $t_P^1 = k_{t,P}^1/k_{t,P}$. The optimization constraint for the selectivities is:

$$\sum_{i}^{n} m_i = 1 \tag{4.17}$$

This model reduces to the ASF distribution model when olefins can not adsorb, i.e. $k_R = 0$. Therefore, eqs 4.7- 4.12 can also be used for the ASF distribution with substitution of $k_R = 0$.

$$\frac{\theta_n}{\theta_{n-1}} = \frac{k_p\theta_M}{k_{t,O}\theta_v + k_{t,P}\theta_H + k_p\theta_M} = \frac{p}{t_O + 1 + p} = \alpha \tag{4.18}$$

The product selectivities are equal to:

$$m_{C_nH_{2n}} = t_O\left(\frac{p}{p + 1 + t_O}\right)^{n-1} = t_O\alpha^{n-1} \tag{4.19}$$

and for paraffins:

$$m_{C_nH_{2n+2}} = \left(\frac{p}{p+1+t_O}\right)^{n-1} = \alpha^{n-1} \tag{4.20}$$

It can easily be seen from eq 4.19 and 4.20 that the predicted olefin to paraffin ratio is equal to t_O and independent of chain length.

The α-olefin readsorption product distribution model (ORPDM) accounts for the chain-length dependent readsorption of olefins on FT sites. The readsorption step depends on carbon number, resulting in a net decrease of the termination to olefins. α_n increases with increasing chain length until no olefins are formed. At high carbon numbers, the chain growth parameter, α_n, approaches a maximum constant value of $\alpha_\infty = p/(1+p)$ (see eq 4.7). The increased readsorption of long-chain olefins results in a decreasing olefin/paraffin ratio with chain length.

4.3 Experimental

Fischer-Tropsch experiments were carried out with a gas-continuous Spinning Basket Reactor (SBR). Details about the experimental set-up, the catalyst, and the analysis sections are described in Chapter 3. The catalyst applied was a commercial precipitated iron catalyst (type LP 33/81) synthesized by Ruhrchemie AG. The baskets were loaded with 2.34 g of unreduced catalyst particles with $0.125 \leq d_P \leq 0.160$ mm. The catalyst was pretreated with hydrogen with a flow rate of 0.83 10^{-3} Nm^3 kg$_{cat}^{-1}$ s^{-1} according to Bukur et al. [40]. The gas space velocity was based on the total mass of the unreduced catalyst. The reactor temperature, T, was increased linearly from 293 K to 553 K by 0.017 K s^{-1}. T remained at 553 K for 24 hours at atmospheric pressure. After reduction, synthesis gas was fed to the reactor at reference conditions of 523 K, 1.50 MPa, F= 2 and a space velocity of 1.51 10^{-3} Nm^3 kg$_{cat}^{-1}$ s^{-1}. Long-chain products have filled the catalyst pores with a liquid phase during the initial stage of the FT experiments.

Liquid products were accumulated in both high-pressure and low-pressure condensers for a typical period of 6-8 hours during steady state of the reactor system. The products were collected and weighed before analysis. Several on-line GC analyses were performed during this period. After changing the process conditions the reactor operated about 24 hours undisturbed before a new mass balance period was started. Deviations of the mass and element balances remained below 5 %.

Reportedly, internal diffusion is insignificant for $d_P < 0.16$ mm [41, 42]. Checking the criteria of Weisz and Prater [43] for the reactants CO and H_2 confirmed that no

intra-particle diffusion limitations could have occurred at even the highest conversion rates observed, and under the conservative assumption that the catalyst pores are filled with long-chain (C_{28}) hydrocarbon waxes.

The experimental conditions were varied as follows: P= 0.8 - 4.0 MPa, F= 0.25 - 4.0, and $\Phi^{in}_{v,0}/W$= 0.5 - 2.0 10^{-3} Nm^3 kg^{-1}_{cat} s^{-1} at a constant temperature of 523 K. The standard deviation of the experimental selectivities was determined for various products by repeating the analysis of the experimental mole fractions:

$$\sigma^2 = \sum_i (m_i - \overline{m})^2/(n-1) < 4\ 10^{-4}\overline{m} \tag{4.21}$$

The reference experiment was repeated 6 times to determine possible deactivation effects on the activity and selectivity of the catalyst. A summary of relevant experimental data is given in Appendix A.

4.4 Results and Discussion

24 kinetic experiments were carried out in the SBR with the Ruhrchemie precipitated iron catalyst at 523 K (see Appendix A). Four experiments were excluded for product distribution modeling due to analytical problems of the on-line analysis of hydrocarbons. Mono-methyl paraffins and β-olefins were below the detection limit in this range and were not taken into account. Potassium promoters in iron catalysts suppress isomerization reactions of α-olefins [20].

Figure 4.3 shows various typical distributions of the hydrocarbon products. Generally, we observed a decrease of the α-olefin/paraffin ratio with increasing carbon number and a curved line for the distribution of paraffins alone and paraffins and olefins combined.

4.4.1 Reactant Composition Effects

Figure 4.4a shows the effect of the (H_2/CO) ratio at the reactor outlet on the hydrocarbon selectivity. The product distribution of the on-line analysis is lumped in three groups of hydrocarbons: methane (w_1), C_2-C_4 (w_{2-4}) (light gases), and C_5-C_{10} (w_{5-10}) (gasoline) and expressed in mass percentages of the on-line analyzed hydrocarbons. In an ideally mixed reactor, the composition at the reactor outlet equals the reactor composition. The feed ratio differs from the exit ratio, due to the stoichiometry of the FT reactions and the water gas shift reaction [14, 44]. The product distribution

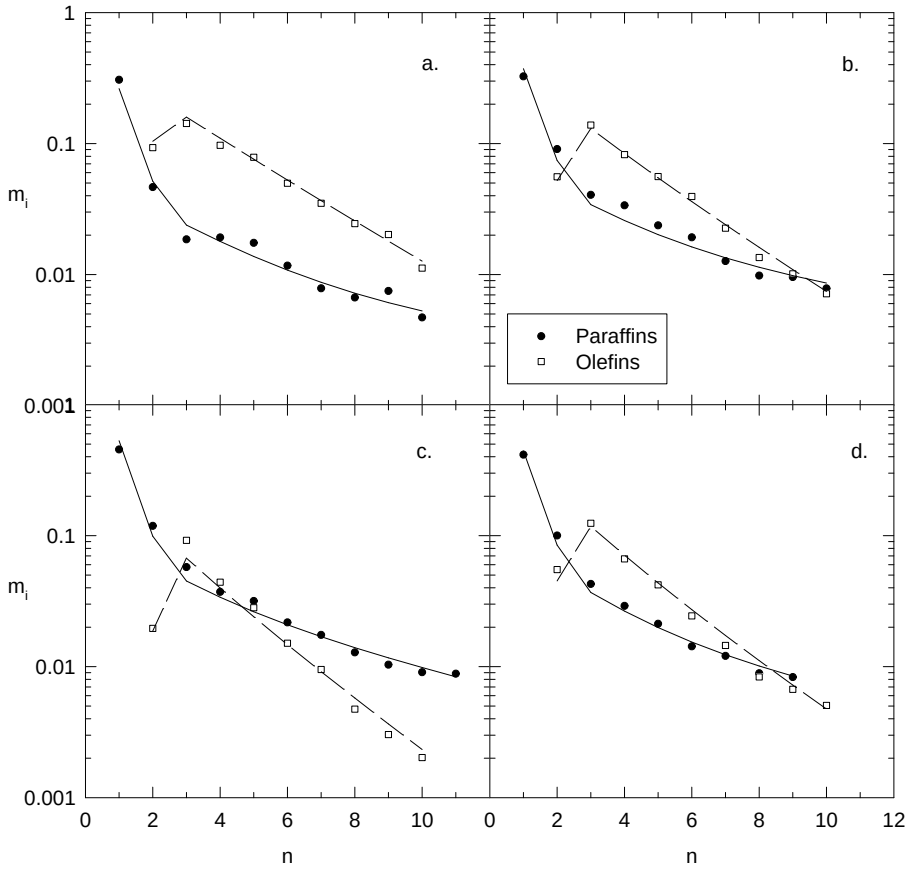

Figure 4.3 Product distribution for various experiments of Appendix A
Experimental conditions:
a. Low H_2/CO feed ratio, P= 1.2 MPa, F= 0.5, $\Phi^{in}_{v,0}/W$= 1.0 10^{-3} Nm^3 kg^{-1} s^{-1} (Run A2).
b. High H_2/CO feed ratio, P= 3.2 MPa, F= 1, $\Phi^{in}_{v,0}/W$= 1.0 10^{-3} Nm^3 kg^{-1} s^{-1} (Run A8).
c. Low space velocity, P= 2.4 MPa, F= 2, $\Phi^{in}_{v,0}/W$= 0.5 10^{-3} Nm^3 kg^{-1} s^{-1} (Run A10).
d: High space velocity, P= 2.4 MPa, F= 2, $\Phi^{in}_{v,0}/W$= 2.0 10^{-3} Nm^3 kg^{-1} s^{-1} (Run A11).
Lines are model ORPDM predictions. Symbols are experimental selectivities.

shifts to lower molecular weight products with an increase of the H_2/CO ratio. Donnelly and Satterfield [20] and Bukur et al. [45] have reported the same effect for the same commercial precipitated iron catalyst.

Figure 4.4b shows that in agreement with Donnelly and Satterfield [20] the olefin content for the light gases decreases sharply from 85 to 45 wt% as the H_2/CO exit ratio increases from 0.5 to 4.5. Low hydrogen concentrations in the feed and in the reactor result in low hydrogen surface concentrations and termination to olefins instead of saturated paraffins. The pressures of both synthesis gas components were varied independently between 0.1 and 1.3 MPa. The measured ratio of the mole fractions of olefin to paraffin (O/P) as function of carbon number for several H_2/CO ratios is shown in Figure 4.5. The O/P ratio shows a minimum at carbon number 2, a maximum for the propene to propane ratio and decreases exponentially. Figure 4.5 shows that the ratio of 1-butene to butane decreased from about 5 to 1 with increasing H_2/CO ratios from 0.5 to 4.5. Similar results were reported by Donnelly and Satterfield [20] and Bukur et al. [45].

4.4.2 Space Velocity Effects

The effect of space velocity on the O/P ratio is plotted in Figure 4.6. The O/P ratio increases with increased space velocity at a H_2/CO feed ratio of 2. The same trend was observed by Dictor and Bell [17] on Fe_2O_3 powders, Bukur et al. [45] on the commercial Ruhrchemie catalyst, and Kuipers et al. [13] on uncoated and wax-coated Co foils. Donnelly and Satterfield [20] found no dependence of the space velocity on the 1-butene to butane ratio in their experiments. Iglesia and co-workers measured the effect of space velocity on the selectivity to olefins and paraffins extensively on Ru-catalysts [36] and Co-catalysts [11]. They observed the olefin selectivities to increase with increasing space velocity, whereas selectivity to paraffins remained constant for C_2 to C_4 and decreased for larger paraffins. Figure 4.7 shows the effect of space velocity on the selectivities of C_1, C_2, and C_4 products. The methane selectivity decreases with increasing space velocity. In agreement with the studies on Co- and Ru- catalysts, olefin selectivities increase with increasing space velocity, while paraffin selectivities decrease. The ethene selectivity increases sharper than the selectivity to ethane decreases. Selectivities of C_4 products show similar behavior. Thus, the decreasing paraffin selectivity cannot result from secondary hydrogenation of olefins alone. The hydrocarbon fraction of C_{20+} consists merely of paraffins, therefore paraffins are formed in primary chain termination reactions. The observed selectivities result from olefin readsorption, causing a decrease of the O/P ratio and increase of the

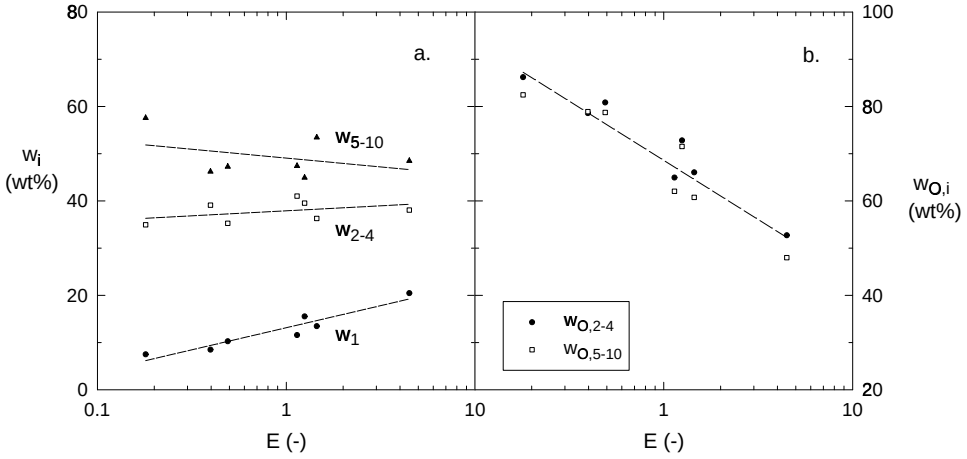

Figure 4.4 Effect of H_2/CO exit ratio (E) on hydrocarbon selectivity (a) and olefin selectivity (b) (T=523 K). Experimental data, see Appendix A.

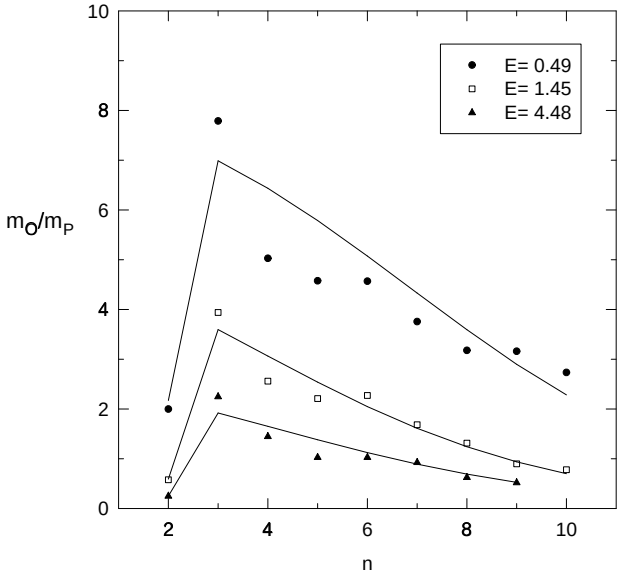

Figure 4.5 Effect of the reactor H_2/CO ratio on molar olefin/paraffin ratio as a function of carbon number. Lines are model predictions with model ORPDM (T=523, $\Phi_{v,0}^{in}/W$= 1.0 10^{-3} Nm^3 kg^{-1} s^{-1}, Run: A2, A3, A4).

chain growth probability [11, 13, 36]. The increasing paraffin selectivity with decreasing space velocity results from an increased surface concentration of (smaller) alkyl chains due to readsorption of olefins.

4.4.3 Product Distribution Models

Both the Anderson-Schulz-Flory (ASF) model as well as the Olefin Readsorption Product Distribution Model (ORPDM) were tested to our experiments at 523 K. The model parameters were optimized for each experiment with the Levenberg-Marquardt method [46].

The ASF model was optimized with two model parameters (p and t_O, see eqs 4.18 - 4.20), within each experiment. The number of parameters in model ORPDM was equal to 7: $p, t_O, k_R, c, t_P^1, t_P^2$, and k_R^2 (see eqs 4.7-4.16). Simultaneous optimization of these parameters within each experiment showed four parameters to be independent of the experimental conditions. The average values of these parameters are shown in Table 4.2. The value of the exponential coefficient c of 0.29 corresponds to the value of 0.30 reported by Iglesia et al. [34] for the dependence of diffusion coefficients and the exponential decrease of the molar O/P ratio with $0.55n$ at 493 K [13].

Introduction of these mean model parameters at 523 K for both the increased readsorption of ethene relative to other olefins and for the termination to C_1 and C_2 products and the exponential increase of the readsorption rate reduces the number of parameters to be optimized from 7 to 3 within each experiment. At high readsorption rates, for example, low space velocity, ($k_R e^{c\ n} \gg 1$) t_O becomes strongly correlated to k_R and cannot be determined separately (see eq 4.12):

$$t_O/(1 + k_R e^{c\ n}) \tag{4.22}$$

In experiments with strongly correlated parameters (t_O and k_R) the ratio of t_O/k_R is

Table 4.2 Optimized model parameters for ORPDM at 523 K that are independent of $\Phi_{v,0}$, P, H_2/CO ratio.

model parameter	value
t_P^1	6.62 ± 1.92
t_P^2	1.59 ± 0.29
k_R^2	$(12.58 \pm 3.55)\ k_R e^{2\ c}$
c	0.29 ± 0.07

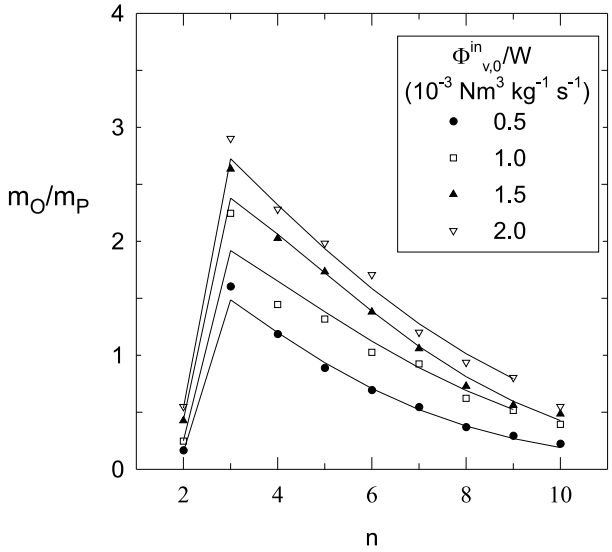

Figure 4.6 Space velocity effects on molar olefin/paraffin ratio as a function of carbon number. Lines are model predictions with model ORPDM (T = 523 K, F = 2, P = 2.4 MPa, Run: A10, A4, A12, A11).

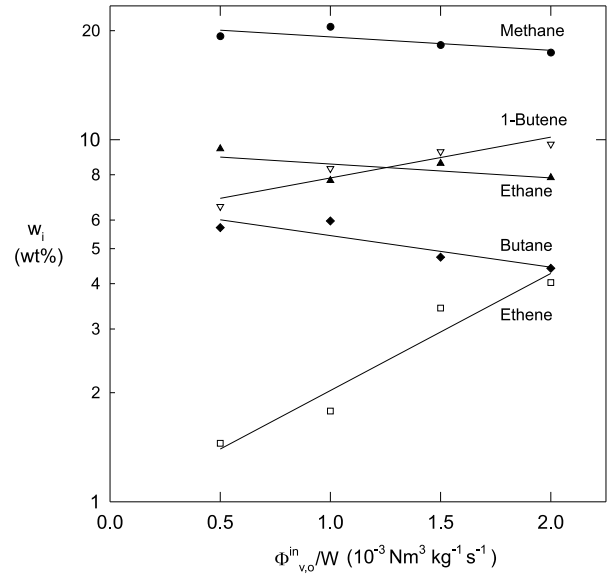

Figure 4.7 Space velocity effects on C_1, C_2, and C_4 selectivity. Experimental conditions, see Figure 4.6.

Table 4.3 Optimized model parameters ORPDM.

Run	p	t_O	k_R	n	s_{rel}
A1	11.64	6.28	0.364	19	9.5
A2	21.40	9.11	0.156	19	11.4
A3	12.55	9.46	0.632	19	6.4
A4	6.97	6.47[1]	–	18	18.6
A6	9.27	7.87	0.500	19	9.4
A8	13.13	7.94	0.457	19	10.5
A9	20.24	7.33	0.123	15	7.5
A10	6.69	4.22[1]	–	20	10.8
A11	9.42	7.73	0.600	18	10.3
A12	6.73	6.91	0.701	19	14.1
A13	7.09	8.20	0.470	19	16.8
A14	8.41	5.74	0.252	20	10.7
A15	6.01	6.53[1]	–	19	10.1
A16	10.19	13.99	0.572	18	13.7
A17	21.23	7.69	0.107	19	10.2
A18	19.46	5.50	0.076	19	14.2
A19	7.18	9.18	0.779	20	7.1
A21	5.00	6.87	1.253	19	11.1
A23	12.92	6.85	0.245	15	7.5
A24	8.29	5.68	0.397	17	9.1

[1] t_O/k_R

modeled. The optimized model parameter values for each experiment are given in Table 4.3.

Table 4.4 shows the accuracies of the optimized models expressed with the relative standard deviation s_{rel} and the $MARR$ function for the paraffins and olefins, respectively, both for the complete set of experimental values at 523 K. The total number of selectivities n as well as the total number of optimized parameters m are also included in this table.

The ASF model observes large deviations between model and experiment. The accuracy of the ASF-model is improved, if hydrocarbons with n= 1-2 are excluded from that model. Figure 4.8a shows a typical product distribution for the on-line hydrocarbon products with the predicted model values with model ASF. The relative residuals of the model appear to be a strong function of the carbon number and product type (see Figure 4.9a). The mean values of the relative residuals ($\overline{RR}$) as a function of

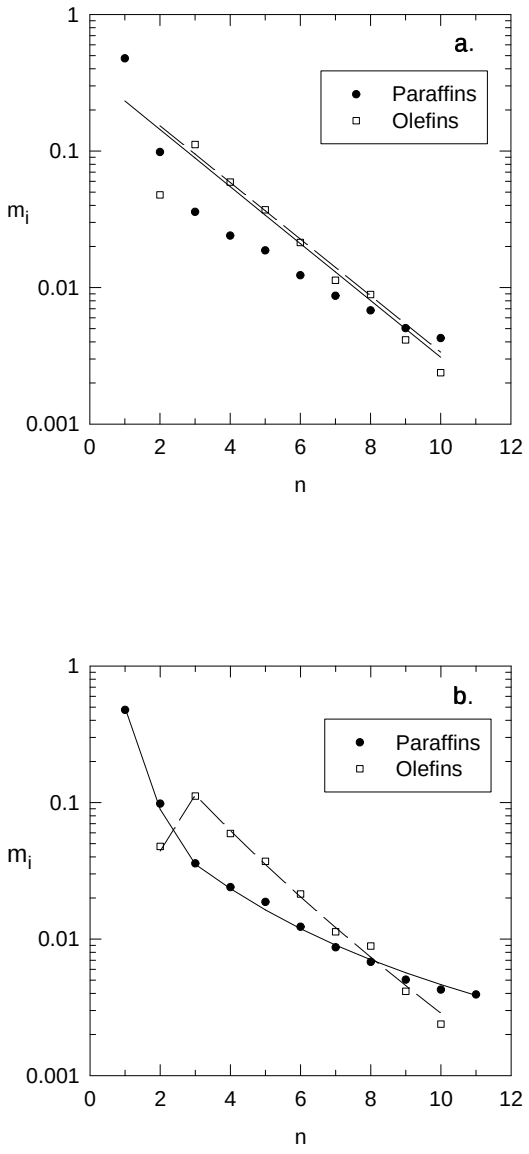

Figure 4.8 Product distribution as a function of carbon number (Run A19: T= 523 K, P= 1.50 MPa, F= 2, $\Phi_{v,0}^{in}/W$= 1.50 10^{-3} Nm^3 kg^{-1} s^{-1}). Lines are model predictions. Symbols are experimental selectivities. a) Model ASF; b) Model ORPDM (p=7.18, t_O=9.18, k_R=0.779).

Table 4.4 Accuracies of the Product Distribution Models.

Model	$MARR$ %		s_{rel} %	n	m
	paraffins	olefins			
ASF	49.9	42.5	70.1	370	40
ORPDM	10.1	9.1	13.3	370	57

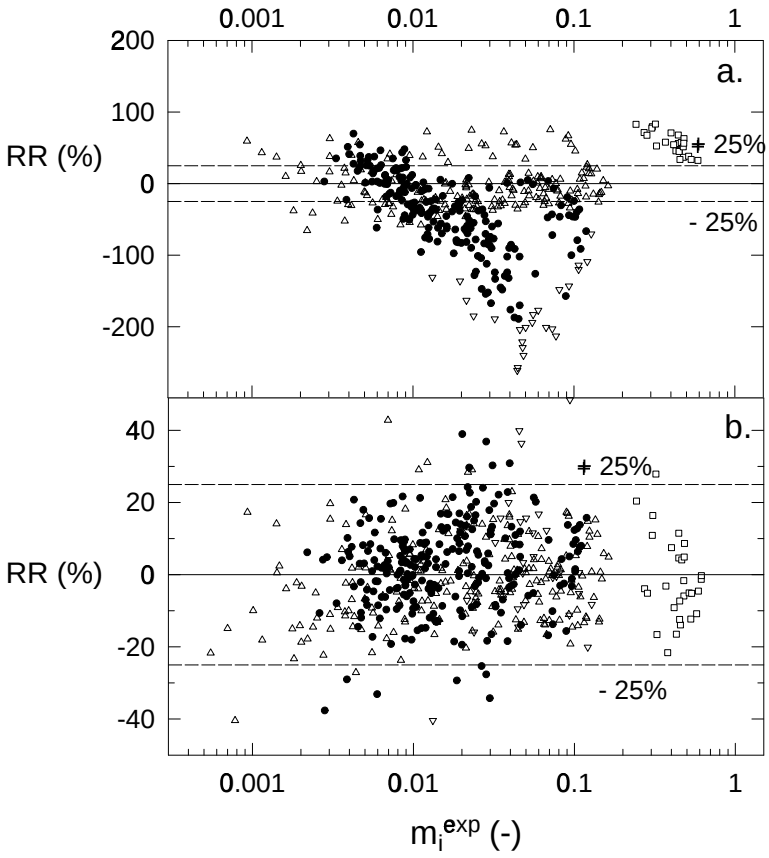

Figure 4.9 Relative residuals versus experimental selectivities. (●: paraffins, □: methane, △: olefins, ▽: ethene) a) Model ASF. b) Model ORPDM.

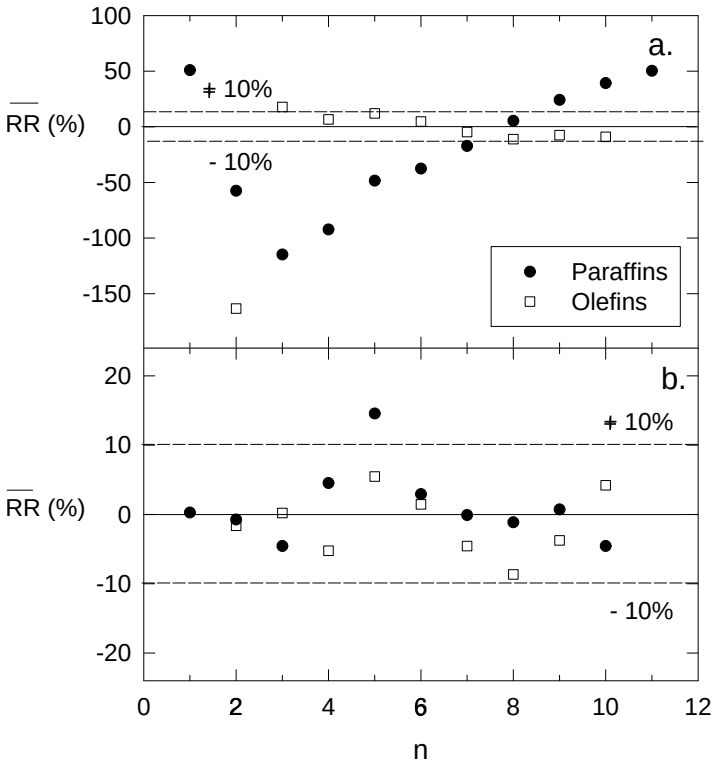

Figure 4.10 Mean relative residuals versus carbon number. a) Model ASF; b) Model ORPDM.

carbon number are plotted in Figure 4.10a. The ASF model appears to give a strong deviation for the selectivity to methane and ethene. Furthermore, a significant trend in the mean deviations of paraffins as function of carbon number was observed (Figure 4.10a). Also, the curved paraffin distribution cannot be described with the ASF model.

The Olefin Readsorption Product Distribution Model, ORPDM, describes n-dependent readsorption of olefins, resulting in a curved distribution of paraffins and a decreasing O/P ratio with carbon number. Examples of product distributions with the predicted model values from model ORPDM are shown in Figure 4.3a-d and 4.8b. The modeled product distribution shows a good prediction of the experimental selectivities. The deviations for C_1 and C_2 products, as well as the increasing paraffin

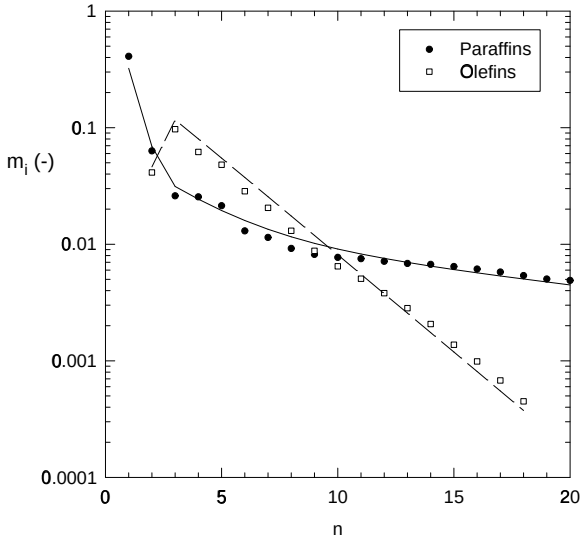

Figure 4.11 Product distribution. Symbols are experimental selectivities of on-line and off-line products. Lines are model predictions of model ORPDM (Run A1: T= 523 K, P= 1.50 MPa, F= 2, $\Phi^{in}_{v,0}/\,W$= 1.50 10^{-3} Nm^3 kg^{-1} s^{-1}).

content of the products are described accurately. The predicted O/P ratios for several experiments are plotted in Figure 4.5 and 4.6. The O/P ratio follows the experimental values accurately, with the exception of n= 3. The model underestimates the O/P ratio slightly at this carbon number.

Figure 4.9b shows that the relative residuals between model ORPDM and experiment are almost always within 25 %, while the mean RR shows no significant trend with carbon number (see Figure 4.10b). The observed deviations from the ASF model are accurately described by our model, resulting in a lower relative variance (s_{rel}= 13.3 %) relative to the ASF model (s_{rel}= 70.1 %) . The accuracy of the new model is demonstrated in Figure 4.11. Here, the hydrocarbon distribution obtained from taking both the on-line and off-line products into account, is compared with model ORPDM. This figure shows that the optimal values of the model parameters are not affected when taking the off-line product composition into account.

The model parameters of model ORPDM are pseudo kinetic rate constants, incorporating true kinetic rate constants, surface concentrations of intermediates, hydrogen

Table 4.5 Effect of process variables on model parameters.

Parameter	Power law
k_R	$3.3210^{-4}\dfrac{P_{H_2}^{1.4}P_{CO}^{-0.49}}{\Phi_{v,0}/W}$
t_O	$6.1686P_{H_2}^{-0.5}$
p	$13.8P_{H_2}^{-0.47}P_{CO}^{0.43}$

Pressures in MPa, $\Phi_{v,0}/W$ in $Nm^3\ kg^{-1}\ s^{-1}$

and vacant sites. Therefore, the model parameters vary with the adjusted process variables, P_{CO}, P_{H_2}, and space velocity. The effect of process variables on the model parameters is shown in Table 4.5. The model parameters, p and k_R were fitted to the experimental conditions with appropriate empirical equations. If it is assumed that the hydrogen adsorption is dissociative [3]:

$$H_2 + 2s \underset{\leftarrow}{\rightarrow} 2Hs \quad (K_{H_2}) \tag{4.23}$$

the relative olefin termination probability, t_O, can be expressed as:

$$t_O = \frac{k_{t,O}\theta_v}{k_{t,P}\theta_H} = \frac{k_{t,O}}{k_{t,P}K_{H_2}^{0.5}P_{H_2}^{0.5}} \propto P_{H_2}^{-0.5} \tag{4.24}$$

The ratio of the termination rates to olefins and paraffins (t_O) decreases with increasing H_2 pressure, whereas the ratio of the chain growth rate to the paraffin termination rate (p) increases with CO pressure and decreases with H_2 pressure. These observations correspond with the experimental results discussed above. The readsorption parameter, k_R, increases with increasing H_2 pressure and decreases with increasing CO pressure and space velocity. CO inhibits readsorption rates, while a high H_2/CO ratio is favorable for readsorption of olefins. The accuracy of the equations presented in Table 4.5 is illustrated in Figure 4.12.

Figure 4.13 shows the effect of carbon number on the chain growth parameter (α_n) calculated with eq 4.6 and 4.7 according to model ORPDM with the optimized parameters from the experiments in Figure 4.5. The chain growth parameter, α_n, is high at $n = 2$ due to rapid readsorption of ethene (k_R^2) and increased termination to C_2 products (t_P^2), minimal for C_3 and increases to the asymptotical value of $\alpha_\infty = p/(1+p)$. Some authors stated that this behavior results from two different catalytic

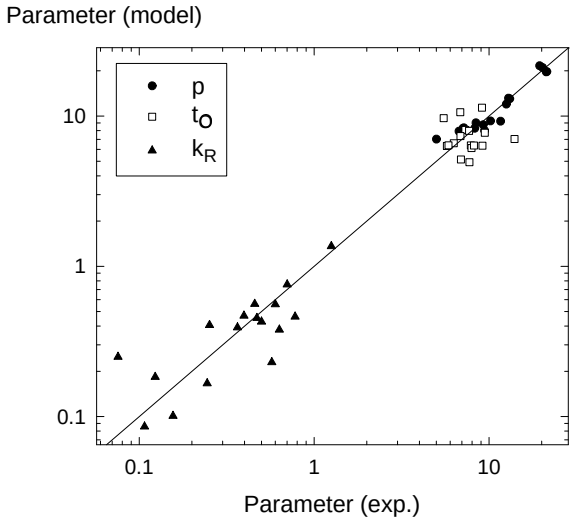

Figure 4.12 Parity graph of experimental (Table 4.3) and modeled parameters (Table 4.5) of model ORPDM.

sites with different chain growth probabilities, since the total hydrocarbon distribution could be fitted by addition of two individual ASF distributions [16, 18, 19]. However such a double-α model cannot explain the following experimental results observed both by us and by, for example, Donnelly and Satterfield [20]: 1) Decrease of the O/P ratio with increasing carbon number. 2) Decrease of the O/P ratio with decreasing space velocity. 3) Decrease of the O/P ratio and mean carbon number with increasing H_2/CO ratios.

Comparison between the model proposed by Zimmerman et al. [21] and ORPDM shows the following major differences: 1) The model of Zimmerman et al. [21] does not account for the increase of the physisorption strength with carbon number. Several studies showed that even in gas-solid reactors, without solubility effects, strong chain length dependencies occur [7, 13]; 2) The strong deviations of C_1 and C_2 products relative to the other hydrocarbons are described accurately with our model in comparison to the model of Zimmerman et al. [21]; 3) Our model describes the complete product distribution accurately without the assumption of secondary hydrogenation on separate hydrogenation sites; 4) ORPDM is tested for a large number of experiments at industrially relevant process conditions, whereas the model of Zimmerman et al. [21]

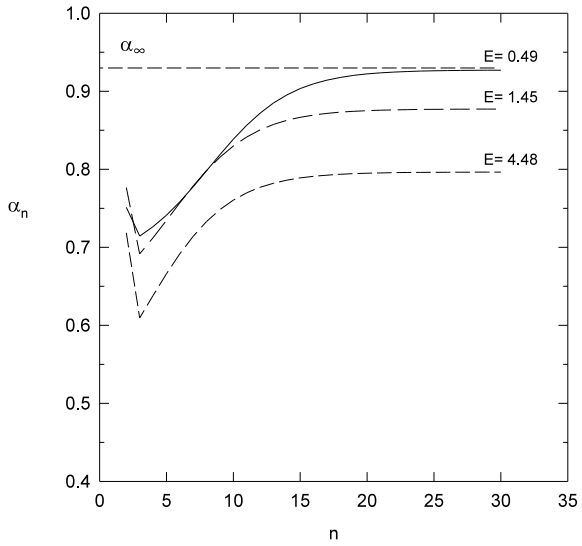

Figure 4.13 Chain growth parameter as function of carbon number. Lines are model predictions of model ORPDM for experiments mentioned in Figure 4.5.

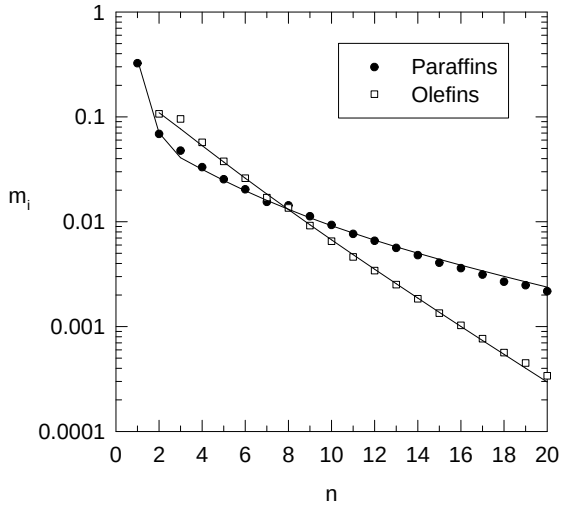

Figure 4.14 Selectivity for Fe-Cu-K (T= 489K, P= 1.62 MPa, H_2/CO=2), data from Madon et al. [35]. Lines are model predictions of model ORPDM ($p = 9.15, t_O = 4.12, k_R = 0.66, c = 0.19, t_P^1 = 4.78, t_P^2 = 1.31, k_R^2 = 1.69e^{2\,c}$).

has been tested for one experiment only.

To check model ORPDM further, we applied it to interpret selectivity data given by Madon et al. [35] for a Fe-Cu-K precipitated catalyst in a fixed bed plug flow reactor. The selectivity data for paraffins and olefins with the optimized values with model ORPDM are given in Figure 4.14. Our readsorption model proves to describe the observed product distribution accurately. The optimal exponential factor, c, of the readsorption term in eq 4.7 on Fe of 0.19 at T= 489 K is lower than the optimized factor in the current study (c= 0.29 at T= 523 K). The asymptotical value of α on Fe appears to be α_∞= 0.901.

ORPDM accounts for secondary readsorption of α-olefins on iron catalysts. In contrast to iron, cobalt catalysts can easily hydrogenate olefins in a secondary reaction [9, 13]. In general, the extent of secondary reactions increases in the order: Fe, Ru, Co [35, 36]. Because of the relatively low tendency of Fe to catalyze secondary hydrogenation, high olefin yields can be obtained with alkali promoted iron catalysts. The present model is applicable for catalysts with no catalytic activity for secondary hydrogenation. However, the model can easily be extended to reaction networks including secondary hydrogenation.

4.5 Conclusions

A new product distribution model, which accounts for n-dependent olefin readsorption, proves to be able to describe accurately the deviations in the observed product distributions, obtained on a precipitated iron catalysts in a gas-solid spinning basket reactor, in both olefins and paraffins from ASF distributions: i.e., a relatively high yield of methane, a relatively low yield of ethene and an exponential decrease of the olefin to paraffin ratio and change of the chain growth parameter with chain length.

For each experimental product distribution three parameters (p, t_O, and k_R) were optimized containing kinetic parameters and surface concentrations of intermediates and vacant sites, whereas four model parameters (c, t_P^1, t_P^2, and k_R^2) were optimized for the entire set of experiments. The effects of the process conditions on the product selectivity and model parameters were investigated. The model parameters could be described successfully with equations depending only on the experimental conditions.

The superior accuracy of the new model in predicting experimentally observed product distributions is obtained from adding one extra parameter only (k_R) in comparison to the Anderson-Schulz-Flory model, without assuming of multiple catalytic chain growth sites.

References

[1] Adesina, A.A., Hydrocarbon synthesis via Fischer-Tropsch reaction: travails and triumphs, *Appl. Catal. A* **1996**, *138*, 345–367.

[2] Anderson, R.B., *Catalysts for the Fischer-Tropsch synthesis*, vol. 4, Van Nostrand Reinhold, New York **1956**.

[3] Bell, A.T., Catalytic synthesis of hydrocarbons over group VIII metals. A discussion on the reaction mechanism, *Catal. Rev.-Sci. Eng.* **1981**, *23*, 203–232.

[4] Dry, M.E., The Fischer-Tropsch synthesis, in J.R. Anderson; M. Boudart, eds., *Catalysis-Science and technology*, vol. 1, Springer-Verlag, New York, 1981 pp. 160–255.

[5] Glebov, L.S.; Kliger, G.A., The molecular weight distribution of the products of the Fischer-Tropsch synthesis, *Russ. Chem. Rev.* **1994**, *63*, 185–194.

[6] Wojciechowski, B.W., The kinetics of the Fischer Tropsch synthesis, *Catal. Rev.-Sci. Eng.* **1988**, *30*, 629–702.

[7] Komaya, T.; Bell, A.T., Estimates of rate coefficients for elementary processes occurring during Fischer-Tropsch synthesis over Ru/TiO_2, *J. Catal.* **1994**, *146*, 237–248.

[8] Schulz, H.; Van Steen, E.; Claeys, M., Olefin formation, hydrogenation and isomerization in the kinetic regime of Fischer-Tropsch synthesis, in *Selective hydrogenation and dehydrogenation*, DGMK, Kassel, Germany, 1993 .

[9] Kuipers, E.W.; Scheper, C.; Wilson, J.H.; Oosterbeek, H., Non-ASF product distributions due to secondary reactions during Fischer-Tropsch synthesis, *J. Catal.* **1996**, *158*, 288–300.

[10] Novak, S.; Madon, R.J.; Suhl, H., Models of hydrocarbon product distributions in Fischer-Tropsch synthesis, *J. Chem. Phys.* **1981**, *74*, 6083–6091.

[11] Iglesia, E.; Reyes, S.C.; Soled, S.L., Reaction-transport selectivity models and the design of Fischer-Tropsch catalysts, in E.R. Becker; C.J. Pereira, eds., *Computer-aided design of catalysts*, Marcel Dekker, New York, 1993 pp. 199–257.

[12] Iglesia, E.; Reyes, S.C.; Madon, R.J.; Soled, S.L., Selectivity control and catalyst design in the Fischer-Tropsch synthesis: sites, pellets, and reactors, in E.E. Eley; H. Pines; P.B. Weisz, eds., *Advances in Catalysis*, vol. 39, Academic Press, New York, 1993 pp. 221–302.

[13] Kuipers, E.W.; Vinkenburg, I.H.; Oosterbeek, H., Chain length dependence of α-olefin readsorption in Fischer-Tropsch synthesis, *J. Catal.* **1995**, *152*, 137–146.

[14] Satterfield, C.N.; Huff, Jr., G.A., Carbon number distribution of Fischer-Tropsch products formed on an iron catalyst in a slurry reactor, *J. Catal.* **1982**, *73*, 187–197.

[15] König, L.; Gaube, J., Fischer-Tropsch-Synthese. Neuere Untersuchungen und Entwickelungen, *Chem.-Ing.-Tech.* **1983**, *55*, 14–22.

[16] Huff, Jr., G.A.; Satterfield, C.N., Evidence for two chain growth probabilities on iron catalysts in the Fischer-Tropsch synthesis, *J. Catal.* **1984**, *85*, 370–379.

[17] Dictor, R.A.; Bell, A.T., Fischer-Tropsch synthesis over reduced and unreduced iron oxide catalysts, *J. Catal.* **1986**, *97*, 121–136.

[18] Egiebor, N.O.; Cooper, W.C.; Wojciechowski, B.W., Carbon number distribution of Fischer-Tropsch CO-hydrogenation products from precipitated iron catalysts, *Can. J. Chem. Eng.* **1985**, *63*, 826–834.

[19] Donnelly, T.J.; Yates, I.C.; Satterfield, C.N., Analysis and prediction of product distributions of the Fischer-Tropsch synthesis, *Energy Fuels* **1988**, *2*, 734–739.

[20] Donnelly, T.J.; Satterfield, C.N., Product distributions of the Fischer-Tropsch synthesis on precipitated iron catalysts, *Appl. Catal. A* **1989**, *52*, 93–114.

[21] Zimmerman, W.H.; Bukur, D.B.; Ledakowicz, S., Kinetic model of Fischer-Tropsch selectivity in the slurry phase, *Chem. Eng. Sci.* **1992**, *47*, 2707–2712.

[22] Krishna, K.R.; Bell, A.T., Estimates of the rate coefficients for chain initiation, propagation, and termination during Fischer-Tropsch synthesis over Ru/TiO_2, *J. Catal.* **1993**, *139*, 104–118.

[23] Schulz, H.; Beck, K.; Erich, E., Kinetics of Fischer-Tropsch selectivity, *Fuel Process. Technol.* **1988**, *18*, 293–304.

[24] Tau, L.-M.; Dabbagh, A.; Davis, B.H., Fischer-Tropsch synthesis: ^{14}C tracer study of alkene incorporation, *Energy Fuels* **1990**, *4*, 94–99.

[25] Breman, B.B.; Beenackers, A.A.C.M.; Rietjens, E.W.J.; Stege, R.J.H., Gas-liquid solubilities of carbon monoxide, carbon dioxide, hydrogen, water, 1-alcohols ($1 \leq n \leq 6$), and n-paraffins ($1 \leq n \leq 6$) in hexadecane, octacosane, 1-hexadecanol, phenantrene, and tetraethylene glycol at pressures up to 5.5 MPa and temperatures from 293 to 552 K, *J. Chem. Eng. Data* **1994**, *39*, 647–666.

[26] Chappelow, C.C.; Prausnitz, J.M., Solubilities of gases in high-boiling hydrocarbon solvents, *AIChE J.* **1974**, *20*, 1097–1103.

[27] Donohue, M.C.; Shah, D.S.; Connally, K.G.; Venkatachalam, V.R., Henry's constants for C_5 to C_9 hydrocarbons in C_{10} and larger hydrocarbons, *Ind. Eng. Chem. Fundam.* **1985**, *24*, 241–246.

[28] Caldwell, L.; van Vuuren, D.S., On the formation and composition of the liquid

phase in Fischer-Tropsch reactors, *Chem. Eng. Sci.* **1986**, *41*, 89–96.

[29] Ruthven, D.M., *Principles of adsorption and adsorption processes*, Wiley & Sons, New York **1984**.

[30] Rybolt, T.R.; Wall, M.D.; Thomas, H.E.; Bramblett, J.W.; Phillips, M., Gas-solid chromatography and virial analysis of hydrocarbon adsorption on 13X zeolite, *J. Colloid Interface Sci.* **1990**, *138*, 113–121.

[31] Keldsen, G.L.; Nicholas, J.B.; Carrado, K.A.; Winans, R.E., Molecular modeling of the enthalpies of hydrocarbons on smectite clay, *J. Phys. Chem.* **1994**, *98*, 279–284.

[32] Miyabe, K.; Suzuki, M., Chromatographic study on liquid-phase adsorption on octadecylsilyl-silica gel, *AIChE J.* **1995**, *41*, 548–558.

[33] Miyabe, K.; Suzuki, M., Solvent effect on adsorption phenomena in reversed-phase liquid chromatography, *AIChE J.* **1995**, *41*, 536–547.

[34] Iglesia, E.; Reyes, S.C.; Madon, R.J., Transport-enhanced α-olefin readsorption pathways Ru-catalyzed hydrocarbon synthesis, *J. Catal.* **1991**, *129*, 238–256.

[35] Madon, R.J.; Iglesia, E.; Reyes, S.C., Non-Flory product distributions in Fischer-Tropsch synthesis catalyzed by Ruthenium, Cobalt, and Iron, in S.L. Suib; M.E. Davis, eds., *Selectivity in Catalysis*, ACS Symposium Series, American Chemical Society, 1993 pp. 382–396.

[36] Madon, R.J.; Reyes, S.C.; Iglesia, E., Primary and secondary reaction pathways in ruthenium-catalyzed hydrocarbon synthesis, *J. Phys. Chem.* **1991**, *95*, 7795–7804.

[37] Madon, R.J.; Iglesia, E., The importance of olefin readsorption and H_2/CO reactant ratio for hydrocarbon chain growth on ruthenium catalysts, *J. Catal.* **1993**, *139*, 576–590.

[38] Erkey, C.; Rodden, J.B.; Akgerman, A., Diffusivities of synthesis gas and n-alkanes in Fischer-Tropsch wax, *Energy Fuels* **1990**, *4*, 275–276.

[39] Reid, R.C.; Prausnitz, J.M.; Poling, B.E., *The properties of gases and liquids*, McGraw-Hill, New York, fourth edn. **1987**.

[40] Bukur, D.B.; Nowicki, L.; Manne, R.K.; Lang, X., Activation studies with a precipitated iron catalyst for Fischer-Tropsch synthesis 2. Reaction studies, *J. Catal.* **1995**, *155*, 366–375.

[41] Post, M.F.M.; van't Hoog, A.C.; Minderhoud, J.K.; Sie, S.T., Diffusion limitations in Fischer-Tropsch catalysts, *AIChE J.* **1989**, *35*, 1107–1114.

[42] Zimmerman, W.H.; Bukur, D.B., Effect of particle size on the activity of a fused iron Fischer-Tropsch catalyst, *Ind. Eng. Chem. Res.* **1989**, *28*, 406–413.

[43] Westerterp, K.R.; van Swaaij, W.P.M.; Beenackers, A.A.C.M., *Chemical reactor design and operation*, Wiley & Sons, second edn. **1984**.

[44] Nettelhoff, H.; Kokuun, R.; Ledakowicz, S.; Deckwer, W.-D., Studies on the kinetics of Fischer-Tropsch synthesis in slurry phase, *Ger. Chem. Eng.* **1985**, *8*, 177–185.

[45] Bukur, D.B.; Patel, S.A.; Lang, X., Fixed bed and slurry reactor studies of Fischer-Tropsch synthesis on precipitated iron catalyst, *Appl. Catal. A* **1990**, *61*, 329–349.

[46] Press, W.H.; Flannery, B.P.; Teukolsky, S.A.; Vetterling, W.T., *Numerical recipes in Pascal*, Cambridge University Press, New York **1989**.